Size-activity threshold of titanium dioxide-supported Cu cluster in CO oxidation

Wasim Ullah Khan[a], Iris K. M. Yu[b,c], Yuqing Sun[b], Matthew I. J. Polson[d], Vladimir Golovko[d], Frank L. Y. Lam[e], Isao Ogino[f], Daniel C. W. Tsang[b,*], Alex C. K. Yip[a]

[a] Department of Chemical and Process Engineering, University of Canterbury, Christchurch 8140, New Zealand

[b] Department of Civil and Environmental Engineering, The Hong Kong Polytechnic University, Hong Kong, China

[c] Department of Chemistry and Catalysis Research Center, Technische Universität München, Lichtenbergstrasse 4, Garching, 85748, Germany

[d] School of Physical and Chemical Sciences, University of Canterbury, Christchurch 8140, New Zealand

[e] Department of Chemical and Biological Engineering, The Hong Kong University of Science and Technology, Hong Kong, China

[f] Division of Applied Chemistry, Faculty of Engineering, Hokkaido University, Sapporo, Japan

*Corresponding author: dan.tsang@polyu.edu.hk (D. C. W. Tsang)

Abstract

Development of non-noble metal cluster catalysts, aiming at concurrently high activity and stability, for emission control systems has been challenging because of sintering and overcoating of clusters on the support. In this work, we reported the role of well-dispersed copper nanoclusters supported on TiO_2 in CO oxidation under industrially relevant operating conditions. The catalyst containing 0.15 *wt.*% Cu on TiO_2 (0.15CT) exhibited a high dispersion (59.1%), a large specific surface area (381 m^2/g_{Cu}), a small particle size (1.77 nm), and abundant active sites (75.8% Cu_2O). The CO oxidation activity measured by the turnover frequency (TOF) was found to be enhanced from 0.60×10^{-3} to 3.22×10^{-3} $mol_{CO} \cdot mol_{Cu}^{-1} \cdot s^{-1}$ as the copper loading decreased from 5 to 0.15 *wt.*%. A CO conversion of approximately 60% was still observed in the supported cluster catalyst with a Cu loading of 5 *wt.*% at 240 °C. No deactivation was observed for catalysts with low copper loading (0.15 and 0.30CT) after 8 h of time-on-stream, which compares favorably with less stable Au cluster-based catalysts reported in the literature. In contrast, catalysts with high copper loading (0.75 and 5CT) showed deactivation over time, which was ascribed to the increase in copper particle size due to metal cluster agglomeration. This study elucidated the size-activity threshold of TiO_2-supported Cu cluster catalysts. It also demonstrated the potential of the supported Cu cluster catalyst at a typical temperature range of diesel engines at light-load. The supported Cu cluster catalyst could be a promising alternative to noble metal cluster catalysts for emission control systems.

Keywords: Pollution control; Copper nanoclusters; CO oxidation; Size-dependent activity; Solid catalyst.

Capsule: Cu clusters show superior catalytic activity in CO oxidation than Cu nanoparticles, which is strongly dependent on the degree of dispersion on the support material.

1. Introduction

The industrial growth, urbanization, and ever-increasing demand for transport vehicles in recent decades have caused detrimental impacts on the environment. Along with catalytic converters in cars, many industrial combustion processes have made significant contributions to global emissions, particularly when it comes to toxic pollutants such as carbon monoxide (CO), nitrogen oxides (NO_x), and unburned hydrocarbons [1]. Among these pollutants, CO is of particular concern because of its toxic nature as an odorless, noxious gas [2]. It can be fatal to both humans and animals. Almost one million children under the age of five die annually due to CO-enriched smoke from household solid fuel combustion, as reported by the World Health Organization (WHO) [3].

In confined environments, CO is generated from household fuels for cooking or heating purposes, and from second-hand smoke emitted from cigarettes [4]. To eliminate CO indoors, ventilation, air purification, and direct removal using low-cost adsorbents, such as activated carbon, have been reported [4]. However, the high electricity costs and complex design involved in ventilation, limited durability and adsorption capacity of the adsorbents, and frequent replacement of filters in air purification equipment limit the application of these methods. Low/medium-temperature catalytic oxidation of CO to CO_2 is an attractive technology in automotive emission abatement because the low energy input enables its use in the advanced combustion engines with low exhaust temperature. Nevertheless, conventional catalysts, such as noble or transition metal nanoparticles, show declining activity at low temperatures because of the high activation energy and catalyst contamination with CO [5-17].

Metal nanoclusters have attracted considerable interest in recent years, mainly due to their size-dependent electronic properties and corresponding unique catalytic activity [18-24]. Metal nanoclusters occupy a niche between larger metallic nanoparticles (used in industrial heterogeneous catalysis) and individual metal ions (*e.g.*, active sites within industrial

homogeneous catalysts), offering an opportunity to explore the unique catalytic performance of clusters in contrast with bulk-like metal particles. Furthermore, with these ultra-small entities, spectroscopic studies and calculations can be utilized to develop an understanding of the fundamentals [25] and mechanisms of oxidation reactions, such as CO oxidation [23]. The distinctive electronic structure of ultra-small atomically precise metal clusters significantly contributes to their strongly size-dependent and often superior catalytic activity [24, 26, 27]. Noble metal nanoclusters, such as Au and Ag, have shown superior catalytic activity in CO oxidation at temperatures as low as 140 K [28-32]; however, the high cost and low abundance limit commercial applications of these metals [33-39].

Copper nanoclusters are a promising alternative due to the low cost and ease of controlled synthesis [40-42]. For example, Vajda *et al*. demonstrated an improved reactivity of copper clusters in the hydrogenation of CO_2 to methanol [43, 44]. Furthermore, ultra-small Cu-oxo clusters can also show unprecedented catalytic activity, as for example, in the oxidation of methane to methanol [45, 46]. Among Cu nanoclusters, hexameric Cu_6 nanoclusters (CuNCs) stand out due to facile synthesis with high yields of clusters [47]. Due to the excellent affinity for CO, CuNCs are investigated in this study for CO oxidation in which the chemisorption of CO is the required elementary step. Titanium dioxide or titania (TiO_2) is one of the most promising supports for heterogeneous catalysts due to its significant reducibility, low toxicity, environmental friendliness, low cost. TiO_2 has a great potential in many emerging applications, such as supercapattery electrode and photocatalytic duet reactions [48, 49]. Particularly, the non-toxic nature, mechanical strength, and good stabilities under oxidative, acidic, and hydrothermal conditions render TiO_2 optimum support for anchoring CuNCs and, thus, maintaining the metal dispersion under working conditions. Moreover, TiO_2 is also known for promoting the activity of gold (Au) nanoparticles/clusters through the formation of Au-TiO_2

interface and enhancement of the size-dependent electronic properties, which contribute towards catalytic performance [20, 50].

So far, TiO_2-supported CuNCs catalysts and their catalytic efficiency in CO oxidation, a key reaction in automotive emission abatement, is not reported in the literature. Nolan (2017) reported that the typical exhaust gas temperatures from a diesel engine ranges from 500 to 700 ℃ at 100% load, and 200 to 300 ℃ with light-load [51]. The developed catalyst system in this work is investigated in the temperature range of 100 to 240 ℃, which lies within the light-load temperature range. Hence, it could be a competitive option for automotive emission abatement. We herein hypothesize that the rate of CO oxidation related with $CO/O_2/CO_2$ adsorption-desorption is strongly dependent on the size, structure, speciation, and stability of the Cu cluster [11-13, 52-57], which are regulated by the Cu loading. It is noteworthy that the catalytic activity generally increases with decreasing metal particle size up to a certain limit, below which catalytic activity may decrease [58, 59]. Changing the particle size may alter the metal-support interface, which affects catalytic activity-controlling factors, including metal-support interactions, surface structures, oxidation and electronic states, and active surface oxide layer [59]. Moreover, under catalytic reaction conditions, nanocluster size and distribution are affected by the presence of the reactant gases [60], such as CO leading to restructuring of nanoclusters, as well as metal particle sintering that leads to catalyst deactivation [61]. The above scientific questions are thus worth comprehensive investigation.

In this work, TiO_2-supported CuNC (CT) catalysts with different copper contents (0.15 to 5 *wt.*%) were synthesized and tested for CO oxidation. The cluster size-activity threshold and the catalyst durability are specifically elucidated herein. Overall, this study aims at providing insights into the use of metal cluster catalysts in industrial processes that require catalytic CO oxidation, such as the emission abatement in petrochemical industries, CO-coupled NOx reduction, and advanced combustion engines in automobiles.

2. Experimental

2.1 Catalyst preparation

Cu_6 nanoclusters (CuNCs) were synthesized using the procedure reported by Albert *et al*. [47]. In a typical procedure which utilizes Schlenk line technique (under Ar), 0.5 g (0.005 mol) of copper(I) chloride and 1.3 g (0.005 mol) of triphenylphosphine (PPh_3) were added into a Schlenk flask, and subsequently, 10 mL of dry, degassed tetrahydrofuran (THF) was added. A white precipitate formed upon stirring the mixture for 30 min. The mixture was placed in an ice bath and kept under continuous stirring. K-Selectride (5 mL of 1.0 M THF, 0.005 mol) was then added slowly using a syringe. The mixture changed from white to dark red. The mixture was stirred continuously for 1 h after removal from the ice bath. The resulting mixture was filtered (using a funnel filter, porosity 3, with sintered glass disc) and washed with THF (2 × 5 mL). The filtrate was layered with hexanes for crystallization, and later, single crystals were obtained for analysis.

Prior to catalyst synthesis, TiO_2-P25 was pre-treated at 200 ℃ for 5 h under vacuum. To prepare a stock solution of clusters, CuNC were crystallized in a Schlenk flask of known weight under argon; removal of crystallisation solvent allowed measurement of the weight of clusters without exposure to air. Addition of 50 mL of dry and degassed THF yielded a stock solution of known concentration under argon without exposing the clusters to air. A known amount of pre-treated TiO_2-P25 (on the basis of a total catalyst mass of 1.1 g) was added into THF (10 mL) in a Schlenk flask under argon, followed by the addition of a calculated amount of CuNCs stock solution to obtain desired copper loadings (ranging from 0.15 to 5 *wt.*%) assuming complete adsorption of CuNCs. Wet impregnation was carried out by stirring the mixture at room temperature overnight. The catalyst sample was subsequently vacuum-dried to evaporate

the solvent completely. The catalysts were designated xCT, where x represents the copper content (*wt.*%) and CT represents a copper cluster supported on TiO_2-P25.

2.2 Catalyst characterization

The single-crystal X-ray diffraction (SXRD) pattern of a pure copper nanocluster crystal was recorded at 120 K using SuperNova Agilent Technologies. The powder XRD (PXRD) patterns of the catalysts were recorded using the same equipment at room temperature over the 2θ range of 20 – 70° using Cu-Kα radiation ($\lambda = 1.54$ Å). The spent catalysts were analyzed using a Philips PW1700 XRD instrument equipped with a Co-Kα radiation source. The scanning range and step to be used for 2θ were 20 – 80° and 0.05°, respectively. MPI Jade® software was used to analyze the PXRD data. The average crystallite size of copper oxide was calculated using the Scherrer equation ($d = \frac{K\lambda}{\beta Cos\theta}$), where d is the mean crystallite size, K is the dimensionless shape factor, λ is the wavelength, β is the line broadening at the full width at half maximum (FWHM) of the peak, and θ is the Bragg angle.

X-ray photoelectron spectroscopy (XPS) (ESCALAB 250Xi spectrometer, USA) with Al Kα radiation was used to investigate the chemical state of Cu on the sample (0.15CT, 0.75CT, and 5CT) surfaces before and after CO oxidation. Narrow high-resolution scan of Cu2p, was obtained using 25 eV pass energy with a step size of 0.05 eV. The charge effect was corrected by using the C 1s line at 285.0 eV. The obtained spectra were fitted by using a curve-fitting program (XPSPEAK41) and a least-squares procedure with peaks of 30% of the Lorentzian-Gaussian peak shape after subtraction of the Shirley baseline. The component peaks were identified by comparison of their binding energies (BEs) with the reported literature values.

Thermogravimetric analysis (TGA) was carried out using SDT Q600 (Alphatec Systems) supported by TA Instruments Universal Analysis 2000 software, under nitrogen (100 mL/min) from ambient temperature to 500 ℃ at a ramping rate of 10 ℃/min. The thermal stability of

the fresh catalysts was analyzed using a NETZSCH-STA 449 F3 Jupiter TGA under airflow (20 mL/min) and at a ramping rate of 10 ℃/min from ambient temperature to 500 ℃.

Temperature-programmed desorption using CO, O_2, and CO_2 (CO-TPD, O_2-TPD, and CO_2-TPD, respectively) and CO chemisorption measurements were conducted on a BELCAT II chemisorption apparatus. For each measurement, 25 − 30 mg of the sample was pre-treated with high-purity helium (He) at 100 °C for 30 min for CO-, O_2-, and CO_2-TPD and at 150 °C for 30 min for CO chemisorption, followed by cooling to ambient temperature. Then, the probe gas mixture, *i.e.*, 10% CO/He, 5% O_2/He, or 5% CO_2/He, was injected at 30 mL/min for 1 h, followed by a flow of He (30 mL/min) for 30 min to remove any residual probe gas mixture in the sample. The sample was heated to 500 °C in a temperature-controlled furnace with a constant heating rate of 10 °C/min with He at 30 mL/min for CO- and O_2-TPD. For CO_2-TPD, the sample was heated to 400 ℃ instead at the same heating rate and He flow rate. For CO chemisorption, CO was injected in pulses until saturation was reached. The outlet signal was measured by a thermal conductivity detector (TCD).

CO chemisorption analysis, as described above, was used to determine the quantity of active metal per gram of catalyst that is available for reaction. The percent dispersion was defined as the ratio of the available amount to the total amount of active sites times 100%. The active particle size is estimated by geometrical calculations, assuming the crystallite shape is of regular spherical geometry. The measured area, A_m (m^2/g), and the volume (expressed in terms of density, ρ_m) of active metal per gram of sample were used to calculate the average diameter (D) of the active metal particles onto which adsorption occurred ($D = 6/\rho_m A_m$).

The UV-visible diffuse reflectance spectra (UV-Vis DRS) were collected using a Cintra 404 UV-Vis spectrophotometer equipped with an integrating sphere to determine the presence of surface copper clusters and copper oxides.

2.3 Catalytic activity

The CO oxidation reaction was carried out in a stainless-steel tubular reactor containing the catalyst (0.2 g) supported on quartz wool as a packed bed. The reactor temperature was controlled using a resistively heated furnace. The temperature of the catalyst bed was monitored using a K-type thermocouple. The reactant mixture was mixed using digital mass flow controllers (ALICAT Scientific, USA), it contained 1% CO and 10% oxygen balanced with argon, and was fed into the reactor at 20 mL/min. Reaction kinetics were studied by operating the reactor in a differential mode with CO conversion less than 15%. The effect of the partial pressure of CO or O_2 on the reaction rate was studied by adjusting the flow rate of CO or O_2 balanced with Ar. The total flow rate was kept at 20 mL/min. The kinetic experiments were performed by varying the concentration of CO or O_2 in the feed from 1 to 20%. The products and unconverted reactants were measured using an online gas chromatograph (GC) (SRI 8610C, SRI Instruments, USA) equipped with a flame ionization detector (FID) and a thermal conductivity detector (TCD). The details of the GC system, the temperature program used and the detection limits are given in Table S2. The CO conversion, rate of reaction, and turnover frequency (TOF) were calculated using the following equations:

$$CO\ Conversion\ (\%) = \frac{CO_{in} - CO_{out}}{CO_{in}} \times 100 \quad (1)$$

$$Rate\ = \frac{F_{CO}X_{CO}}{m}\ or\ \frac{F_{CO}X_{CO}}{m_{Cu}} \quad (2)$$

$$TOF = \frac{F_{CO}X_{CO}}{n_{Cu}} \quad (3)$$

where F_{CO} is the molar flow rate of CO (mol/s), X_{CO} is the conversion of CO, m and m_{Cu} is the amount of catalyst and copper in the catalyst used (g), n_{Cu} is the number of moles of Cu in the catalyst, the rate of reaction is in $mol_{CO}/s \cdot g_{Cat}$ or $mol_{CO}/s \cdot g_{Cu}$, and TOF is in $(n_{Cu} \cdot s)^{-1}$.

3. Results and Discussion

3.1 Preparation and characterization of hexameric copper nanoclusters

The Cu_6 nanoclusters (CuNCs) were characterized using SXRD by selecting a single crystal in the CuNC sample. The SXRD results of the as-synthesized crystals were compared with those reported in the literature, as shown in Table S1. The obtained crystal structure is different from the reported structure with a higher content of THF, which is the residual solvent from the synthesis and constitutes a part of the cluster structure associated with the ligand. Using the same space group of $P2_1$, the crystal parameters were evaluated as a = 14.2847 (10) Å, b = 16.0082 (10) Å, c = 21.3909 (10) Å, β = 92.1230 (10)°, V = 4888.15 (5) $Å^3$, ρ = 1.369 $g.cm^{-3}$, and μ = 2.716 mm^{-1}. The difference between the literature results [47] and the current findings are attributed to the temperature difference used for SXRD, which was 120 K in our case. The CuNCs were thermally treated under nitrogen when using TGA to estimate the removal and/or thermal stability of organic ligands attached to the copper cluster core. Fig. S1 shows the weight loss versus temperature; it can be seen that the ligand is completely removed at temperatures above 250 °C. A slight weight loss (~3 *wt.*%) is observed initially at approximately 150 °C, which indicates the removal of weakly-bonded THF. This is in agreement with the theoretically calculated weight of 2.7% obtained from 0.75THF according to the formula of CuNCs, *i.e.*, $[(PPh_3)CuH]_6 \cdot 0.75THF$ presented in Table S1, followed by the removal of triphenylphosphine ligand (~75 *wt.*%; theoretically 6 moles of PPh_3 correspond to 80% of the total formula weight) leaving behind Cu cluster cores. The slight increase at the end plateau may be ascribed to nitride formation or oxidation [62]. The as-synthesized CuNCs were then deposited onto TiO_2 and used as a catalyst for CO oxidation.

3.2 Catalyst characterization

To assess the thermal stability and loss of ligand under the catalytic reaction conditions, the same concentration of oxygen (*i.e.*, 10%) was used in the TGA. Fig. S2 shows that heating to 500 °C in the air led to slight weight loss for the 0.15CT (~ 2%) and 0.30CT (4%) catalysts but a significant weight loss in the case of 5CT (27%). The change in weight at or before 120 °C is attributed to the loss of water physically adsorbed on the catalyst surface. The onset temperature for the initial weight loss over all the catalysts is found to be above 200 °C, which implies that the copper cluster is still intact in the "as made" catalysts. A slight increase in weight (0.35%) observed on 5CT at approximately 155 °C could be attributed to the oxidation of surface copper species, which is not apparent in the low-loading catalysts (0.15 and 0.30CT). Comparing the TGA of CuNC with and without the TiO_2 support, it is obvious that the sample of CuNC supported on TiO_2 did not show any weight loss even at 200 °C, while the CuNC without the support had approximately 12% weight loss. This result suggests that the CuNC supported on TiO_2 remained intact at 200 °C. Complete ligand removal was achieved around 376 °C, as evidenced by the onset of a plateau for the 5CT sample. The catalysts showed colour change when exposed to high temperatures under an oxidative environment, which provides an indication of thermal stability. The change in the colour of 5CT catalyst into yellow was evident as compared with no colour change in 0.15CT and 0.30CT catalysts, indicating the latter were more resistant to high temperature. The UV-Vis DRS results (Fig. S3) show similar visible light absorbance spectra (λ ~410 nm) of the bare support and the supported clusters. In particular, a typical surface plasmon resonance peak for nanoparticles at approximately 560 nm was absent from all the spectra, which confirms that copper clusters do not agglomerate to form nanoparticles [63] even at a high Cu loading (*i.e.*, 5CT) in the case of "as made" catalysts.

To identify the nature of the crystalline phase present in the as-synthesized catalysts, PXRD analysis was carried out. The characteristic peaks of copper or copper oxide are not detected (Fig. S4), which is due to the ultra-small size of individual Cu_6 clusters and fine dispersion of

CuNCs over the support surface (*i.e.*, no large crystals of Cu_6 were formed during catalyst fabrication) [64]. The diffraction peaks at 2θ = 25, 37, 48, 54, and 56° are the characteristic peaks of the anatase phase [65], and the peaks at 2θ = 28, 35, 42, and 63° are assigned to the rutile phase of TiO_2 [66]. Further, XPS analysis of Cu2p binding states was performed to determine the oxidation state of Cu at the surface of the as-prepared catalysts (Fig. 1). The Cu 2p3/2 signal at 932.0 eV showed that the surface of the fresh 0.15CT (75.8%) and 0.75CT (72.6%) mainly contained Cu(I) species [67-69]. However, when the Cu content topped at 5 *wt.*%, Cu species on the 5CT surface was predominantly consisted of oxidized Cu form including Cu(II) (933.4 eV, 43.5%) and shake-up CuO (940−945 eV, 20.7%) [64-66]. Thus, lower Cu loading improved the density of active sites (probably Cu_2O) for CO adsorption and oxidation on the catalyst surface.

The particle size, metal dispersion, and metal surface area, which are determined using CO chemisorption, are important factors influencing the catalytic performance. In general, CO and N_2O are used as probe gases to study chemisorption of Cu sites. N_2O chemisorption requires oxygen uptake by Cu^0 sites, and thus, any unreduced Cu sites are not taken into account [70]. Since copper exists in two oxide forms, the reduction of both forms of copper oxide needs to be ensured before oxidizing Cu^0 sites using N_2O. Moreover, reduction of Cu_2O is more difficult than that of CuO [71]. Hence, the variations in (a) the temperature of copper oxide reduction to Cu^0 and (b) the temperature of N_2O reduction, *i.e.*, Cu^0 oxidation to Cu^+, affect the Cu site evaluation. These concerns limit the use of N_2O as a probe gas in our work, and therefore, CO chemisorption was used for Cu site measurements. The chemisorption results in Table 1 show that increasing the Cu loading from 0.15 to 5 *wt.*% led to a decrease in copper dispersion and specific surface area. The 0.15CT catalyst exhibits a Cu dispersion of 59.1%, which is approximately 12 times higher than that of the 5CT catalyst (5.1%). Similarly, Chary et al. (2004) inferred the increase in copper amount from 2.5 to 10 *wt.*% caused a decrease in copper

dispersion from 21.8 to 6.3%, respectively [72]. Findings demonstrated by Baharudin et al. (2019) also revealed that the amount of copper clusters and their pre-treatment conditions (*i.e.*, temperature and time) had significant impact on copper dispersion. They further reported that increasing the amount of copper cluster from 0.5 to 13 *wt.*% drastically reduced the copper dispersion from 41.9% to as low as 1.3% [62]. Furthermore, the average particle diameter for the 0.15CT catalyst (1.77 nm) is approximately 5 times smaller than that of 0.75CT (9.59 nm), and this gap further increases when comparing to 5CT (20.5 nm). These results suggest that both the dispersion and the average particle diameter may play a pivotal role during the reaction.

The nature of the adsorption active sites and the extent of interaction between CO and the catalyst surface were measured using CO-TPD, as shown in Fig. 2a. CO-TPD profiles for all catalysts can be divided into at least two regions, *i.e.*, the low-temperature region (LTR) ranging from 60 to 250 °C and the high-temperature region (HTR) ranging from 250 to 460 °C. In the LTR, CO-TPD for the 0.15CT catalyst exhibited a broader desorption peak at approximately 155 ℃, and this peak shifted to ~175 ℃ when the copper content was increased from 0.15 to 0.75 *wt.*%. The peak maximum is almost the same (~175 ℃) for the 0.75 and 5CT catalysts, which indicates the similar nature of the adsorption sites in these catalysts. The relatively low desorption peak temperature (155 ℃) in 0.15CT implies that easier CO desorption from its surface compared to catalysts with higher Cu loadings. It has been recognized that the desorption peak temperature is related to the activation energy of the desorption and that the heat of adsorption is equivalent to the activation energy of the desorption for a spontaneous adsorption process [62, 73]. The increase in desorption peak temperature from 155 ℃ to 175 ℃ for the 0.75 and 5CT catalysts indicates that these catalysts with higher Cu contents exhibit higher activation energy of CO desorption [74]. Noteworthy, there is a lower temperature shoulder in the profile for the 5CT catalyst, which is observed at

the temperature similar to that of the peak maximum for 0.15CT sample. This could indicate that the 5CT sample has two types of sites capable of desorbing CO at low temperatures.

In the HTR, all the catalysts also exhibited a noticeable peak, which is attributed to predominantly CO adsorption on stronger adsorption sites. The desorption peak temperature follows the same trend as in the LTR and increases from 290 to 305 ℃ when the Cu contents increase from 0.15 to 0.75 *wt.*%. It is noteworthy that the 5CT catalyst exhibited two distinct desorption peaks (*cf*. a peak with a shoulder as in LTR) at approximately 350 and 400 ℃, which can be assigned to the presence of stronger adsorption sites. It is reported that CO hardly adsorbs on pure CuO [75], the adsorption sites in this work can be either Cu^{+} and/or Cu^{0}, with the least possibility of Cu^{2+}. The area under the curve of CO-TPD, which represents the CO coverage, *i.e.*, the amount of CO adsorbed, increases with the increasing copper content (Table 2). For instance, the 0.15CT catalyst showed a CO uptake of 0.103 mmol/g in the LTR, which increased to 0.226 mmol/g for the 5CT catalyst, reflecting the fact that there were more adsorption sites in the latter.

The O_2-TPD results in Fig. 2b shows the adsorption behaviour of oxygen over the catalysts. The catalysts have only one distinct peak in the temperature range of 60 to 310 °C. The 0.15CT catalyst exhibited a broad desorption peak at ~180 ℃. In contrast, the 0.75CT catalyst showed distinct and broader desorption peak at a slightly higher temperature, *i.e.*, 190 ℃, with a shoulder at a lower temperature of ~160 ℃. This characteristic peak can be attributed to the desorption of molecular oxygen species (O_2) adsorbed on the surface [76, 77]. The area under the curve is related to the amount of oxygen adsorbed over the catalyst surface, and it is found that the 0.75CT catalyst exhibits more oxygen adsorption than the 0.15CT catalyst. For instance, an O_2 uptake of 0.194 mmol/g was observed on the 0.75CT catalyst compared to 0.177 mmol/g for the 0.15CT catalyst (Table 2).

The desorption of CO_2 within the reaction temperature range provides insight into the catalyst affinity for the product, an important factor controlling reaction rate and product yield. The CO_2-TPD results show that CO_2 starts desorbing from the surface of 0.30CT and 0.75CT at temperatures as low as 60 ℃ (Fig. S5). Both catalysts exhibit two desorption peaks between 60 and 360℃, which can be divided into two regions: the low-temperature region (LTR, 60 – 250 ℃) and the high-temperature region, (HTR, 250 – 360 ℃). The maximum desorption peak in the LTR shifted from 170 ℃ to 160 ℃ when the Cu loading increased from 0.30 to 0.75 *wt.*%, suggesting the presence of relatively weaker adsorption sites for CO_2 in the 0.75CT compared to 0.30CT. On the other hand, the shift of the maximum desorption peak in the HTR is not obvious, indicating that the CO_2 adsorption sites over 0.30CT and 0.75CT have comparable strength. Table S2 shows that the total amount of CO_2 adsorbed on the 0.30CT and 0.75CT catalysts are 0.244 mmol/g and 0.221 mmol/g, respectively. The lesser amount of CO_2 adsorbed over the 0.75CT catalyst can be ascribed to the fact that CO_2 mainly adsorbs on the oxide support rather than on the Cu-based sites [78, 79]. Overall, it can be concluded that both of these catalysts show the ability to release the CO_2 from the surface within the temperature range of 60 to 360 ℃. Moreover, both catalysts demonstrated a similar amount of CO_2 desorbed from the surface, although CO_2 binds relatively stronger to the surface of the 0.30CT than that of the 0.75CT catalyst.

3.3 CO oxidation reaction and kinetics over xCT catalysts

The catalytic performance of the materials with different copper nanocluster loadings (from 0.15 to 5 *wt.*%) in CO oxidation was measured at atmospheric pressure in the temperature range of 100 – 250 °C, with conversion and TOF graphs shown in Figs. 3a and 3b. The catalytic activity test over the bare TiO_2 support (blank) showed no CO conversion in the abovementioned temperature range. It, therefore, ruled out any catalytic role of the support during the reaction [80]. Moreover, low oxidation state copper species are reported to be

unstable in an oxidative environment [81]. Thus, unsupported CuNCs are not suitable for CO oxidation reactions as very low surface area bulk copper oxides will be formed under reaction conditions. Immobilization of CuNCs would allow the formation of catalysts with exceptionally high dispersion of copper active sites [62, 82, 83]. The catalytic performance in terms of CO conversion versus temperature showed that the activity increased with increasing copper content (Fig. 3a). For instance, at 188 ℃, the 0.15CT catalyst showed CO conversion of approximately 6%, while the 5CT catalyst exhibited a CO conversion more than threefold higher than that of 0.15CT. CuNC anchoring over TiO_2-P25 was so effective that even small contents of copper (0.15 *wt.*%) exhibited noticeable CO conversion (9%) at 240 °C accompanied by the corresponding CO_2 formation. This significant increase in activity can be attributed to the formation of active sites enhancing the conversion of CO into CO_2.

The activity results in terms of turnover frequency (TOF), as shown in Fig. 3b, clearly show that 0.15CT exhibits superior catalytic activity in CO oxidation at 200 °C with a TOF (3.22×10^{-3} $(n_{Cu}\cdot s)^{-1}$) more than 2 times higher than those of 0.30CT (1.41×10^{-3} $(n_{Cu}\cdot s)^{-1}$), 0.75CT (0.75×10^{-3} $(n_{Cu}\cdot s)^{-1}$), and 5CT (0.60×10^{-3} $(n_{Cu}\cdot s)^{-1}$) at 480 min time-on-stream. The results also demonstrate that the stability of the catalysts is strongly dependent on the Cu loading. The 0.15CT and 0.30CT catalysts demonstrated excellent stability for a reaction duration of 480 min, while catalysts with higher Cu loading, *i.e.*, 0.75CT and 5CT catalysts, showed deactivation from 0.75×10^{-3} $(n_{Cu}\cdot s)^{-1}$ to 0.45×10^{-3} $(n_{Cu}\cdot s)^{-1}$ and 0.60×10^{-3} $(n_{Cu}\cdot s)^{-1}$ to 0.03×10^{-3} $(n_{Cu}\cdot s)^{-1}$, respectively. These results suggest that copper loading of 0.30 *wt.*% is the threshold limit for stable catalytic performance. The cause of deactivation is explored by the characterization of the catalysts after the reaction, as discussed in Section 3.4. The results are consistent with those reported by Du *et al*. [12], who investigated the influence of the size of gold nanoparticles, ranging from 2.9 to 5.1 nm, on Au/TiO_2 catalysts for CO oxidation. The catalyst with an average size of 3.8 nm outperformed the same catalysts with average sizes of

2.9 and 5.1 nm. Bond [84] also demonstrated through the compensation plot concept that the size of Au particles influences the activity during CO oxidation reaction. He concluded that most of the particles remain non-metallic for active catalysts, while metallic catalysts tend to show lower catalytic activity.

A kinetic study of the 0.15CT and 0.75CT catalysts was performed at 200 °C. The logarithmic plots of the rate of reaction versus partial pressures of CO and O_2 are shown in Fig. 4a and 4b, respectively. It can be observed that the rate of reaction increased with increase in partial pressures of CO and O_2 in the feed for both the 0.15CT and 0.75CT catalysts. The kinetic orders were found to be 0.22 and 0.37 with respect to CO and O_2, respectively, for the 0.15CT catalyst. In contrast, the 0.75CT catalyst gave CO and O_2 kinetic orders of 0.19 and 0.30, respectively. The Arrhenius plot (Fig. 4c) indicates that the apparent activation energies over the 0.15CT and 0.75CT catalysts are 14.1 and 27.9 kJ/mol, respectively. These activation energies are lower than those reported in the literature for TiO_2-supported Cu catalysts prepared by photo-deposition (ph) and impregnation (imp) techniques (33.1 and 59.2 kJ/mol for Cu-TiO_2-ph and Cu-TiO_2-imp, respectively) [85].

Based on the kinetic results, a reaction mechanism can be proposed for 0.15CT and 0.75CT catalysts. It has been reported in the literature that Mars van-Krevelen and Eley Rideal models present the zero- and first-order reaction, respectively, with respect to O_2 partial pressure [2]. Both the models are inconsistent with the kinetic results in this work, and hence they are not considered. To investigate the role of the lattice oxygen of the reducible TiO_2 support, the catalysts were first tested in a reaction condition with only CO and Ar in the absence of oxygen. No formation of CO_2 was observed despite the small loss of CO due to the chemisorption on the catalysts' surface. The Langmuir-Hinshelwood model relevant to the metal-support interface can be considered in which CO chemisorbs on Cu active sites while O_2 adsorbs on

the support. Both chemisorbed species react on the Cu-TiO_2 interface to form CO_2. The following steps can be proposed:

$$CO + Cu* \underset{k_{-1}}{\overset{k_1}{\leftrightarrow}} CO - Cu* \qquad K_1 = \frac{k_1}{k_{-1}} \tag{4}$$

$$O_2 + TiO_2* \underset{k_{-2}}{\overset{k_2}{\leftrightarrow}} O_2 - TiO_2* \qquad K_2 = \frac{k_2}{k_{-2}} \tag{5}$$

$$CO - Cu* + O_2 - TiO_2* \underset{k_{-3}}{\overset{k_3}{\leftrightarrow}} CO_2 - Cu* + O - TiO_2* \qquad K_3 = \frac{k_3}{k_{-3}} \tag{6}$$

$$CO - Cu* + O - TiO_2* \underset{k_{-4}}{\overset{k_4}{\leftrightarrow}} CO_2 - Cu* + TiO_2* \qquad K_4 = \frac{k_4}{k_{-4}} \tag{7}$$

$$CO_2 - Cu* \underset{k_{-5}}{\overset{k_5}{\leftrightarrow}} CO_2 + Cu* \qquad \frac{1}{K_5} = \frac{k_{-5}}{k_5} \tag{8}$$

where Cu* and TiO_2* represent the vacant sites that are assumed to be constant. Among steps (4) to (8), step (6), *i.e.*, the reaction across the interface between Cu active site (with adsorbed CO) and titania (with adsorbed and activated O_2), is the rate-determining step (RDS). The chemisorption of CO or O_2 cannot be considered the RDS, as this would require rate expression to be first-order kinetics with respect to CO or O_2 [64], which contradicts the kinetic results. The chemisorption of both CO and O_2 is confirmed by CO- and O_2-TPD; however, the CO_2-TPD profiles also corroborate the abovementioned findings. The proposed RDS, assuming that O_2 non-dissociatively chemisorbs over the TiO_2 surface, is consistent with earlier reported results [86]. Based on the elementary steps, the following rate expression is formulated, and details can be seen in S1 in the supporting information.

$$r_{CO2} = k \frac{K_{CO} K_{O_2} [CO] [O_2]}{(1 + K_{CO}[CO])(1 + K_{O_2}[O_2])} \tag{9}$$

To ensure that the surface reaction across Cu-titania interface was indeed the RDS, the rate expression (Eq. 9) was fitted to the initial rate of reaction (IRR) measured at a different initial partial pressure of CO for the 0.15CT and 0.75CT catalysts (Fig. 5). The rate constant, *k*, was

approximately 4.71×10^{-8} and 6.67×10^{-8} mol/s·g_{cat} for the 0.15CT and 0.75CT catalysts, respectively. The experimental data are consistent with the rate equation formulated according to the proposed elementary steps (Eq. 4-8). This result indicates that the CO oxidation reaction catalyzed by the TiO_2-supported Cu cluster catalysts is limited by the surface reaction across Cu-TiO_2 interface and, hence, rules out any role of adsorption or desorption as the RDS. Therefore, it can be concluded that both 0.15CT and 0.75CT catalysts catalyze CO oxidation overall according to the Langmuir-Hinshelwood reaction mechanism with the RDS occurring across the Cu active site and titania support.

3.4 Post-reaction characterization of the catalyst

The CO chemisorption results of the spent catalyst (Table 1) showed a loss of dispersion and an increase in particle size. The dispersion of the 0.15CT catalyst decreased from 59.1% to 53%. The particle size of the 5CT (63.1 nm) catalyst after the reaction increased three times relative to that of the fresh catalyst (20.5 nm) based on modeling using Cu_2O active species, which are present in all spent catalysts. This is ascribed to the thermodynamically favorable interface elimination process, which lowers the surface energy by reducing surface area through agglomeration and, thus, decreases the total free energy of the system.

The XRD patterns of the spent catalysts (Fig. S6) show the presence of copper oxides that are not found in fresh catalysts, confirming the agglomeration of metal particles during the reaction. In addition to typical diffraction profiles of anatase and rutile, peaks for Cu_2O and CuO are also detected. The diffraction peak near 43° is difficult to distinguish between anatase (PDF# 21-1272) and Cu_2O (PDF# 34-1354). It is clear that the CuO (PDF# 44-0706) peak is present in the 0.75CT and 5CT catalysts at a 2-theta of 45°. The XPS analyses of the spent catalysts, particularly the 5CT (no Cu(I) detected), further emphasized that the Cu(I) species was oxidized after catalytic oxidation of CO (Fig. S7).

The surface plasmon resonance (SPR) peak (Fig. S8) for copper nanoparticles is reported to be in the wavelength range of 560 – 760 nm [63] while SPR peaks for pure Cu_2O or CuO correspond to the wavelengths of 600 to 800 nm [87, 72]. The exact position of the SPR peak depends on the size and aspect ratio of the particle. The SPR peak at ~380 nm can be assigned to Cu_2O and/or CuO because these oxides are formed due to the oxidation of CuNCs during the reaction. The formation of Cu_2O nanoparticles, with a diameter of 2 nm, is observed to be appearing at ~370 nm [88]. As indicated in XRD and XPS analyses, all catalysts showed Cu_2O and/or CuO, while none of the catalysts show Cu characteristic peak, which demonstrates that Cu clusters are well dispersed and too small to be detected by XRD or XPS as was the case in the fresh catalyst. The intensity of the SPR peak occurring at 380 nm increases when Cu loading is increased, which shows the concurrent oxidation and sintering of surface Cu clusters. The SPR peak with very weak intensity appearing at 567 nm indicates the presence of a small number of metallic Cu nanoparticles as a result of sintering during the reaction over all the catalysts. The intensity of the SPR peak increases with increasing amounts of copper, suggesting that catalysts with higher copper contents (0.75 and 5 *wt.*%) are more prone to sintering than catalysts with lower loading (0.15 *wt.*%).

As mentioned earlier, pure, unsupported CuNCs and TiO_2-P25 supports cannot convert CO to CO_2. The interface between Cu oxide species and titania is most likely the active center for the reaction to proceed [64, 84, 89]. The Huttig temperature that causes significant mobility of surface atoms is 134 ℃ for copper nanoparticles [90, 91], which is well below the reaction temperature of 200 ℃ in this study. Therefore, surface copper species tend to aggregate at higher copper loadings. Moreover, the Huttig temperature of Cu_2O and CuO is found to be 229 ℃ and 260 ℃, respectively, which are above the reaction temperature [92]. Hence, the oxide particles are relatively less susceptible to aggregation as compared with metallic particles, but the SPR peak intensity suggests otherwise. It can be inferred that the particle diameter,

which is also an influencing factor in the UV-Vis DRS analysis, for copper oxides is large enough to be detected by both XRD and UV-Vis DRS as opposed to particle diameter of metallic Cu which is detected by UV-Vis DRS but not by XRD despite the aggregation. It can also be seen from the CO-TPD results that the amount of CO adsorbed increased with increasing Cu content, which is in agreement with the CO conversion measured over the tested catalysts. The drawback of higher-loading catalysts is their long-term instability, as metal agglomeration increases severely during the reaction.

The characterizations, *e.g.*, UV-Vis DRS and XRD, after the long-term reaction test, also show an increase in metal particle size. It has been reported that a change in particle size affects the oxidation state of copper, which in turn influences the distribution of these oxides on the surface of the catalyst [93]. The presence of CuO in the 0.75CT and 5CT catalysts, as indicated in the XRD and XPS patterns of the used catalysts (Fig. S7 and Fig. S6), is another factor contributing to the decrease in the activity of these catalysts over time because CuO is less active than Cu_2O and Cu^0 for the CO oxidation reaction [94].

Cu nanoparticles and supported noble metals, such as Au, Pd and Pt, are widely reported for CO oxidation reaction [95-104]. The comparison of the rate of reaction (per gram of metal) for the xCT catalysts with the CO oxidation results published in the literature reveals that the xCT catalysts showed an activity (*e.g.*, 5.06×10^{-5} mol/s·g_{Cu} by 0.15CT) exceeding the catalytic activity of expensive catalysts, such as Au clusters supported on TiO_2 (*e.g.*, zero activity by Au_{25}/TiO_2) [25] and Cu supported on metal-organic framework UiO-66 (2.40×10^{-5} mol/s·g_{Cu}) [94], under similar reaction conditions to the ones used in the current study (Table 3). Moreover, the xCT catalysts (*e.g.*, 5.06×10^{-5} mol/s·g_{Cu} by 0.15CT) in this work also outperformed the conventional Cu nanoparticles deposited on SBA-15 (4.18×10^{-5} mol/s·g_{Cu}) [95]. A comprehensive investigation at a molecular level, for example, density functional theory (DFT) calculations, is required to give more insights into the mechanism behind such performance.

4. Conclusions

This study demonstrated the high CO oxidation activity of atomically precise Cu nanoclusters (CuNCs) anchored on TiO_2-P25. The results revealed the significance of interfacial active sites and the size-activity threshold for copper loading content between 0.15 and 5 *wt.*%. The excellent dispersion, high copper surface area, and more intensive active sites (*i.e.*, Cu_2O), as determined by CO chemisorption, UV-Vis DRS, XRD, and XPS, remained to be the key factors behind the stable catalytic performance of catalysts with lower Cu loading. The 0.15CT and 0.30CT catalysts remained stable over the 8 h time-on-stream, revealing the upper copper loading activity threshold at 0.3 *wt.*% as catalysts with higher loadings deactivated quickly and significantly. The stability of these catalysts was assigned to the smaller particle size, higher dispersion, and significantly lower content of active sites at the surface of the support, which prevented particle agglomeration and growth. In contrast, 0.75CT and 5CT catalysts showed metal sintering, which eventually resulted in catalyst deactivation. The metal particle sintering was further confirmed by post-reaction CO chemisorption, UV-Vis DRS, and XRD. The presence of CuO was found to be another factor affecting the deactivation of the catalysts over time. The kinetic study revealed that the 0.15CT and 0.75CT catalysts followed the Langmuir-Hinshelwood mechanistic model. The RDS was suggested to be across the interface boundary reaction of CO adsorbed onto Cu active sites with oxygen species adsorbed on titania, as confirmed by the experimental data obtained regarding initial reaction rates at various CO partial pressures. The apparent activation energies were 14.1 and 27.9 kJ/mol for the 0.15CT and 0.75CT catalyst, respectively, while the reaction orders with respect to CO and O_2 were 0.22 and 0.37, respectively, for the 0.15CT catalyst and 0.19 and 0.30, respectively, for the 0.75CT catalyst. Importantly, our Cu_6-based catalysts demonstrated reaction rates (per gram of metal) comparable to the rates obtained using gold-based materials, which are both more

expensive and less abundant. These results showed the important role of the support and appropriately low metal cluster loading needed to ensure long enough distances between active sites (Cu cluster-derived species) required to guarantee high dispersion and small particle size for concurrently achieving excellent activity and thermal durability, which is currently a formidable challenge in the field of CO oxidation. The developed Cu-cluster catalysts exhibited a long-term catalytic stability, indicating a potential application in automobile emission abatement, such as that in the catalytic converter of vehicles. Future studies on the recyclability, reactivation of the supported Cu-clusters, and the impact of other emission gases, including NO_x, water vapors, hydrocarbons etc., on the clusters activity will be useful to extend the applications beyond automobile emission abatement.

Acknowledgments

The authors would like to thank the financial support from the Ministry of Business, Innovation & Employment in New Zealand under the MBIE Endeavour "Smart Ideas" grant (UOCX1905), Hong Kong Research Grants Council (PolyU 15217818), and the publication scholarship offered by the College of Engineering at the University of Canterbury.

References

[1] R.M. Heck, R.J. Farrauto, Automobile exhaust catalysts, Appl. Catal. A-Gen. 221 (2001) 443–457.

[2] S. Royer, D. Duprez, Catalytic Oxidation of Carbon Monoxide over Transition Metal Oxides, Chemcatchem 3 (2011) 24–65.

[3] B. Gordon, Mackay, R., Rehfuess, E., Inheriting the World: the Atlas of Children's Health and the Environment WHO, (2004).

[4] P.W. Seo, H.J. Choi, S.I. Hong, S.C. Hong, A study on the characteristics of CO oxidation at room temperature by metallic Pt, J. Hazard. Mater. 178 (2010) 917–925.

[5] K. Wong, Q. Zeng, A. Yu, Interfacial synergistic effect of the Cu monomer or CuO dimer modified CeO_2(111) catalyst for CO oxidation, Chem. Eng. J. 174 (2011) 408–412.

[6] Z.Q. Zou, M. Meng, L.H. Guo, Y.Q. Zha, Synthesis and characterization of $CuO/Ce_{1-x}Ti_xO_2$ catalysts used for low-temperature CO oxidation, J. Hazard. Mater. 163 (2009) 835–842.

[7] A.K. Srivastava, A. Saxena, D. Shah, T.H. Mahato, B. Singh, A.R. Shrivastava, P.K. Gutch, C.P. Shinde, Catalytic removal of carbon monoxide over carbon supported palladium catalyst, J. Hazard. Mater. 241 (2012) 463–471.

[8] C.H. Tseng, T.C.K. Yang, H.E. Wu, H.C. Chiang, Catalysis of oxidation of carbon monoxide on supported gold nanoparticle, J. Hazard. Mater. 166 (2009) 686–694.

[9] S.H. Xie, H.X. Dai, J.G. Deng, H.G. Yang, W. Han, H. Arandiyan, G.S. Guo, Preparation and high catalytic performance of Au_3DOM Mn_2O_3 for the oxidation of carbon monoxide and toluene, J. Hazard. Mater. 279 (2014) 392–401.

[10] F.F. Han, Y.H. Yang, J.Y. Han, O.Y. Jin, N. Na, Room-temperature cataluminescence from CO oxidation in a non-thermal plasma-assisted catalysis system, J. Hazard. Mater. 293 (2015) 1–6.

[11] F. Yang, M.S. Chen, D.W. Goodman, Sintering of Au Particles Supported on TiO_2(110) during CO Oxidation, J. Phys. Chem. C 113 (2009) 254–260.

[12] M.M. Du, D.H. Sun, H.W. Yang, J.L. Huang, X.H. Jing, T. Odoom-Wubah, H.T. Wang, L.S. Jia, Q.B. Li, Influence of Au Particle Size on Au/TiO_2 Catalysts for CO Oxidation, J. Phys. Chem. C 118 (2014) 19150–19157.

[13] Tana, F. Wang, H. Li, W. Shen, Influence of Au particle size on Au/CeO_2 catalysts for CO oxidation, Catal. Today 175 (2011) 541–545.

[14] N.S. Portillo-Vélez, R. Zanella, Comparative study of transition metal (Mn, Fe or Co) catalysts supported on titania: Effect of Au nanoparticles addition towards CO oxidation and soot combustion reactions, Chem. Eng. J. 385 (2020) 123848.

[15] F. Wang, K. Zhao, H. Zhang, Y. Dong, T. Wang, D. He, Low temperature CO catalytic oxidation over supported Pd–Cu catalysts calcined at different temperatures, Chem. Eng. J. 242 (2014) 10–18.

[16] Y. Park, S.K. Kim, D. Pradhan, Y. Sohn, Surface treatment effects on CO oxidation reactions over Co, Cu, and Ni-doped and codoped CeO_2 catalysts, Chem. Eng. J. 250 (2014) 25–34.

[17] D.I. Potemkin, P.V. Snytnikov, V.D. Belyaev, V.A. Sobyanin, Preferential CO oxidation over Cu/CeO_{2-x} catalyst: Internal mass transport limitation, Chem. Eng. J. 176–177 (2011) 165–171.

[18] X. Liu, D. Astruc, Atomically precise copper nanoclusters and their applications, Coordin. Chem. Rev. 359 (2018) 112–126.

[19] M. Turner, V.B. Golovko, O.P.H. Vaughan, P. Abdulkin, A. Berenguer-Murcia, M.S. Tikhov, B.F.G. Johnson, R.M. Lambert, Selective oxidation with dioxygen by gold nanoparticle catalysts derived from 55-atom clusters. Nature 454 (2008) 981–984.

[20] D.P. Anderson, J.F. Alvino, A. Gentleman, H. Al Qahtani, L. Thomsen, M.I.J. Polson, G.F. Metha, V.B. Golovko, G.G. Andersson, Chemically-synthesised, atomically-precise gold clusters deposited and activated on titania. Phy. Chem. Chem. Phy. 15 (2013) 3917–3929.

[21] B.G. Donoeva, D.S. Ovoshchnikov, V.B. Golovko, Establishing a Au Nanoparticle Size Effect in the Oxidation of Cyclohexene Using Gradually Changing Au Catalysts. ACS Catal. 3 (2013) 2986–2991.

[22] R.H. Adnan, G.G. Andersson, M.I.J. Polson, G.F. Metha, V.B. Golovko, Factors influencing the catalytic oxidation of benzyl alcohol using supported phosphine-capped gold nanoparticles. Catal. Sci. Technol. 5 (2015) 1323–1333.

[23] P. Poldorn, Y. Wongnongwa, S. Namuangruk, N. Kungwan, V.B. Golovko, B. Inceesungvorn, S. Jungsuttiwong, Theoretical mechanistic study of CO catalytic oxidation by O_2 on an ultra-small 13-atom bimetallic Ag_7Au_6 cluster. Appl. Catal. A: Gen. 595 (2020) 117505.

[24] Y. Du, H. Sheng, D. Astruc, M. Zhu, Atomically Precise Noble Metal Nanoclusters as Efficient Catalysts: A Bridge between Structure and Properties, Chem. Rev. 120 (2020) 526–622.

[25] M. Walter, J. Akola, O. Lopez-Acevedo, P.D. Jadzinsky, G. Calero, C.J. Ackerson, R.L. Whetten, H. Grönbeck, H. Häkkinen, A unified view of ligand-protected gold clusters as SUPERATOM complexes, PNAS 105 (2008) 9157–9162.

[26] B.C. Gates, M. Flytzani-Stephanopoulos, D.A. Dixon, A. Katz, Atomically dispersed supported metal catalysts: perspectives and suggestions for future research, Catal. Sci. Technol. 7 (2017) 4259.

[27] A. Halder, L.A. Curtiss, A. Fortunelli, S. Vajda, Perspective: size selected clusters for catalysis and electrochemistry. J. Chem. Phys. 148 (2018) 110901.

[28] M. Lamoth, M. Plodinec, L. Scharfenberg, S. Wrabetz, F. Girgsdies, T. Jones, F. Rosowski, R. Horn, R. Schlögl, E. Frei, Supported Ag Nanoparticles and Clusters for CO Oxidation: Size Effects and Influence of the Silver–Oxygen Interactions, ACS Appl. Nano Mater. 2 (2019) 2909–2920.

[29] X.T. Nie, H.F. Qian, Q.J. Ge, H.Y. Xu, R.C. Jin, CO Oxidation Catalyzed by Oxide-Supported $Au_{25}(SR)_{18}$ Nanoclusters and Identification of Perimeter Sites as Active Centers, ACS Nano, 6 (2012) 6014–6022.

[30] X.T. Nie, C.J. Zeng, X.G. Ma, H.F. Qian, Q.J. Ge, H.Y. Xu, R.C. Jin, CeO_2-supported $Au_{38}(SR)_{24}$ nanocluster catalysts for CO oxidation: a comparison of ligand-on and -off catalysts, Nanoscale 5 (2013) 5912–5918.

[31] A. Sanchez, S. Abbet, U. Heiz, W.-D. Schneider, H. Häkkinen, R.N. Barnett, U. Landman, When Gold Is Not Noble: Nanoscale Gold Catalysts, J. Phys. Chem. A 103 (1999) 9573–9578.

[32] B. Yoon, H. Häkkinen, U. Landman, A.S. Wörz, J.-M. Antonietti, S. Abbet, K. Judai, U. Heiz, Charging Effects on Bonding and Catalyzed Oxidation of CO on Au_8 Clusters on MgO, Science 307 (2015) 403–407.

[33] S. Fernandez-Garcia, S.E. Collins, M. Tinoco, A.B. Hungria, J.J. Calvino, M.A. Cauqui, X.W. Chen, Influence of {111} nanofaceting on the dynamics of CO adsorption and oxidation over Au supported on CeO_2 nanocubes: An operando DRIFT insight, Catal. Today 336 (2019) 90–98.

[34] U. Goswami, S. Basu, A. Paul, S.S. Ghosh, A. Chattopadhyay, White light emission from gold nanoclusters embedded bacteria, J. Mater. Chem. C 5 (2017) 12360–12364.

[35] H. Kondoh, R. Toyoshima, Y. Monya, M. Yoshida, K. Mase, K. Amemiya, B.S. Mun, In situ analysis of catalytically active Pd surfaces for CO oxidation with near ambient pressure XPS, Catal. Today 260 (2016) 14–20.

[36] J.P.H. Li, Z.B. Liu, H. Wu, Y. Yang, Investigation of CO oxidation over Au/TiO_2 catalyst through detailed temperature programmed desorption study under low temperature and Operando conditions, Catal. Today 307 (2018) 84–92.

[37] Q.F. Yao, X. Yuan, V. Fung, Y. Yu, D.T. Leong, D.E. Jiang, J.P. Xie, Understanding seed-mediated growth of gold nanoclusters at molecular level, Nat. Commun. 8 (2017).

[38] L. Shang, S.J. Dong, G.U. Nienhaus, Ultra-small fluorescent metal nanoclusters: Synthesis and biological applications, Nano Today 6 (2011) 401–418.

[39] B.Y. Wu, C.W. Wang, P.C. Chen, H.T. Chang, Glutathione assisted preparation of gold nanoclusters using minimum amount of protein, Sensor. Actuat. B-Chem. 238 (2017) 1258–1265.

[40] X.H. Gao, S.J. He, C.M. Zhang, C. Du, X. Chen, W. Xing, S.L. Chen, A. Clayborne, W. Chen, Single Crystal Sub-Nanometer Sized $Cu_6(SR)_6$ Clusters: Structure, Photophysical Properties, and Electrochemical Sensing, Adv. Sci. 3 (2016).

[41] S. Shahsavari, I.M. Oskouie, S.H. Ghazvini, M. Hasany, F.H. Saboor, A. Simchi, A.L. Rogach, Ligand functionalized copper nanoclusters for versatile applications in catalysis, sensing, bioimaging, and optoelectronics, Mater. Chem. Front. 3 (2019) 2326–2356.

[42] Z.G. Wang, Y. Xiong, S.V. Kershaw, B.K. Chen, X.M. Yang, N. Goswami, W.F. Lai, J.P. Xie, A.L. Rogach, In Situ Fabrication of Flexible, Thermally Stable, Large-Area, Strongly Luminescent Copper Nanocluster/Polymer Composite Films, Chem. Mater. 29 (2017) 10206–10211.

[43] C. Liu, B. Yang, E. Tyo, S. Seifert, J. DeBartolo, B. von Issendorff, P. Zapol, S. Vajda, L.A. Curtiss, Carbon Dioxide Conversion to Methanol over Size-Selected Cu_4 Clusters at Low Pressures. J. Am. Chem. Soc. 137 (2015) 8676–8679.

[44] B. Yang, C. Liu, A. Halder, E.C. Tyo, A.B.F. Martinson, S. Seifert, P. Zapol, L.A. Curtiss, S. Vajda, Copper Cluster Size Effect in Methanol Synthesis from CO_2, J. Phys. Chem. C 121 (2017) 10406–10412.

[45] T. Ikuno, J. Zheng, A. Vjunov, M. Sanchez-Sanchez, M.A. Ortuño, D.R. Pahls, J.L. Fulton, D.M. Camaioni, Z. Li, D. Ray, B.L. Mehdi, N.D. Browning, O.K. Farha, J.T. Hupp, C.J. Cramer, L. Gagliardi, J.A. Lercher, Methane Oxidation to Methanol Catalyzed by Cu-Oxo Clusters Stabilized in NU-1000 Metal–Organic Framework, J. Am. Chem. Soc. 139 (2017) 10294–10301.

[46] K.D. Vogiatzis, G. Li, E.J.M. Hensen, L. Gagliardi, E.A. Pidko, Electronic Structure of the $[Cu_3(\mu\text{-}O)_3]^{2+}$ Cluster in Mordenite Zeolite and Its Effects on the Methane to Methanol Oxidation, J. Phys. Chem. C 121 (2017) 22295−22302.

[47] C.F. Albert, P.C. Healy, J.D. Kildea, C.L. Raston, B.W. Skelton, A.H. White, Lewis-Base Adducts of Group-11 Metal(I) Compounds .49. Structural Characterization of Hexameric and Pentameric (Triphenylphosphine)Copper(I) Hydrides, Inorg. Chem. 28 (1989) 1300–1306.

[48] I. Heng, F.W. Low, C.W. Lai, J.C. Juan, N. Amin, S.K. Tiong, High performance supercapattery with rGO/TiO_2 nanocomposites anode and activated carbon cathode, J. Alloys Compd. 796 (2019) 13–24.

[49] K. Shichijo, M. Fujitsuka, Y. Hisaeda, H. Shimakoshi, Visible light-driven photocatalytic duet reaction catalyzed by the B12-rhodium-titanium oxide hybrid catalyst, J. Organomet. Chem. 907 (2020) 121058.

[50] M. Chen and D.W. Goodman, Catalytically active gold on ordered titania supports, Chem. Soc. Rev. 37 (2008) 1860–1870.

[51] D.P. Nolan, Chapter twelve- Classified Area Pump Installations, in: D.P. Nolaan (Ed.), Fire Pump Arrangements at Industrial Facilities (Third Edition). Gulf Professional Publishing, 2017, pp. 161–167.

[52] M. Bowker, Q.M. Guo, Y.X. Li, R.W. Joyner, Structure Sensitivity in Co Oxidation over Rhodium, Catal. Lett. 18 (1993) 119–123.

[53] B. Atalik, D. Uner, Structure sensitivity of selective CO oxidation over Pt/gamma-Al_2O_3, J. Catal. 241 (2006) 268–275.

[54] W.Y. Song, E.J.M. Hensen, Structure Sensitivity in CO Oxidation by a Single Au Atom Supported on Ceria, J. Phys. Chem. C 117 (2013) 7721–7726.

[55] Y. He, J.C. Liu, L.L. Luo, Y.G. Wang, J.F. Zhu, Y.G. Du, J. Li, S.X. Mao, C.M. Wang, Size-dependent dynamic structures of supported gold nanoparticles in CO oxidation reaction condition, P. Natl. Acad. Sci. USA 115 (2018) 7700–7705.

[56] C.S. Chen, J.H. You, J.H. Lin, Y.Y. Chen, Effect of highly dispersed active sites of Cu/TiO_2 catalyst on CO oxidation, Catal. Commun. 9 (2008) 2381–2385.

[57] M.A. Nygren and P.E.M. Siegbahn, Theoretical Study of Chemisorption of CO on Copper clusters, J. Phys. Chem. 96 (1992) 7579–7584.

[58] B. Roldan Cuenya, Synthesis and catalytic properties of metal nanoparticles: Size, shape, support, composition, and oxidation state effects, Thin Solid Films, 518 (2010) 3127–3150.

[59] N.K. Soliman, Factors affecting CO oxidation reaction over nanosized materials: A review, J. Mater. Res. Technol. 8 (2019) 2395–2407.

[60] L. Liu, D.N. Zakharov, R. Arenal, P. Concepcion, E.A. Stach, A. Corma, Evolution and stabilization of subnanometric metal species in confined space by in situ TEM, Nat. Commun. 9 (2018) 574.

[61] E. Vesselli, M. Peressi, Nanoscale Control of Metal Clusters on Templating Supports, in: P. Fornasiero, M. Cargnello (Eds.), Studies in Surface Science and Catalysis, Elsevier, 2017, pp. 285–315.

[62] L. Baharudin, A.C.K. Yip, V.B. Golovko, M.I.J. Polson, M.J. Watson, CO temperature-programmed desorption of a hexameric copper hydride nanocluster catalyst supported on functionalized MWCNTs for active site characterization in a low-temperature water–gas shift reaction, Chem. Eng. J., 377 (2019) 120278.

[63] R. Li, S.K. Wu, X.Y. Wan, H.X. Xu, Y.J. Xiong, Cu/TiO_2 octahedral-shell photocatalysts derived from metal-organic framework@semiconductor hybrid structures, Inorg. Chem. Front. 3 (2016) 104–110.

[64] J.Q. Lu, C.X. Sun, N. Li, A.P. Jia, M.F. Luo, Kinetic study of CO oxidation over CuO/MO_2 (M = Si, Ti and Ce) catalysts, Appl. Surf. Sci. 287 (2013) 124–134.

[65] Y.L. Yu, Y. Tang, J.X. Yuan, Q. Wu, W.J. Zheng, Y.A. Cao, Fabrication of N-TiO_2/$InBO_3$ Heterostructures with Enhanced Visible Photocatalytic Performance, J. Phys. Chem. C 118 (2014) 13545–13551.

[66] Y.L. Yu, J.S. Wang, W. Li, W.J. Zheng, Y. Cao, Doping mechanism of Zn^{2+} ions in Zn-doped TiO_2 prepared by a sol-gel method, Crystengcomm, 17 (2015) 5074–5080.

[67] Y. Gao, L. Zhang, A. J. van Hoof, E.J. Hensen, On the surface-dependent oxidation of Cu_2O during co oxidation: Cu^{2+} is more active than Cu^{+}, Appl. Catal. A: Gen., 602 (2020), 117712.

[68] W.T. Yang, C.J. Lin, T. Montini, P. Fornasiero, S. Ya, S.Y.H. Liou, High-performance and long-term stability of mesoporous Cu-doped TiO_2 microsphere for catalytic CO oxidation, J. Hazard. Mater., 403 (2020), 123630.

[69] Z. Wan, Y. Sun, D.C.W. Tsang, K.M. Iris, J. Fan, J.H. Clark, Y. Zhou, X. Cao, B. Gao, Y.S. Ok, A sustainable biochar catalyst synergized with copper heteroatoms and CO_2 for singlet oxygenation and electron transfer routes, Green Chem., 21 (2019), 4800–4814.

[70] A. Dandekar, R.T.K. Baker, M.A. Vannice, Carbon-supported copper catalysts I. Characterization, J. Catal. 183 (1999) 131–154.

[71] J.Y. Kim, J.A. Rodriguez, J.C. Hanson, A.I. Frenkel, P.L. Lee, Reduction of CuO and Cu_2O with H_2: H embedding and kinetic effects in the formation of suboxides, J. Am. Chem. Soc. 125 (2003) 10684–10692.

[72] K.V.R. Chary, K.K. Seela, G.V. Sagar, B. Sreedhar, Characterization and Reactivity of Niobia Supported Copper Oxide Catalysts, J. Phys. Chem. B 108 (2004) 658–663.

[73] V. Rakić and L. Damjanović Temperature-Programmed Desorption (TPD) Methods, in: Auroux A. (eds) Calorimetry and Thermal Methods in Catalysis, 154 (2013) pp. 131–174.

[74] D. Murzin and T. Salmi, Dynamic Catalysis, in: Catalytic Kinetics, Elsevier Science, (2005) pp. 285–339.

[75] S. Varghese, M. G. Cutrufello, E. Rombi, C. Cannas, R. Monaci and I. Ferino, CO oxidation and preferential oxidation of CO in the presence of hydrogen over SBA-15-templated CuO-Co_3O_4 catalysts, Appl. Catal., A 443–444 (2012) 161–170.

[76] Q. Liang, X. Wu, D. Weng, H. Xu, Oxygen activation on Cu/Mn–Ce mixed oxides and the role in diesel soot oxidation, Catal. Today 139 (2008) 113–118.

[77] Y. Zeng, T. Wang, S. Zhang, Y. Wang, Q. Zhong, Sol–gel synthesis of CuO-TiO_2 catalyst with high dispersion CuO species for selective catalytic oxidation of NO, Appl. Surf. Sci. 411 (2017) 227–234.

[78] D. Chen, D. Mao, G. Wang, X. Guo, J. Yu, CO_2 hydrogenation to methanol over CuO-ZnO-ZrO_2 catalyst prepared by polymeric precursor method, J. Sol-gel Sci. Technol. 89 (2019) 686–699.

[79] K.K. Bando, K. Sayama, H. Kusama, K. Okabe, H. Arakawa, In–situ FT–IR study on CO_2 hydrogenation over Cu catalysts supported on SiO_2, $A1_2O_3$, and TiO_2. Appl. Catal. A: Gen. 165 (1997) 391–409.

[80] O.H. Laguna, J.J. Murcia, H. Rojas, C. Jaramillo-Paez, J.A. Navio, M.C. Hidalgo, Differences in the Catalytic Behavior of Au-Metalized TiO2 Systems During Phenol Photo-Degradation and CO Oxidation, Catalysts 9 (2019) 331.

[81] C. Barriere, K. Piettre, V. Latour, O. Margeat, C.O. Turrin, B. Chaudret, P. Fau, Ligand effects on the air stability of copper nanoparticles obtained from organometallic synthesis, J. Mater. Chem. 22 (2012) 2279–2285.

[82] L. Baharudin, A.C.K. Yip, V.B. Golovko, M.I.J. Polson, K.-F. Aguey-Zinsou, M.J. Watson, CO oxidation and the inhibition effects of carboxyl-modification and copper clusters on multi-walled carbon nanotubes, Appl. Catal. B: Environ. 262 (2020) 118265.

[83] L. Baharudin, I. Severinsen, A.C.K. Yip, V.B. Golovko, M.J. Watson, Kinetics and constraints of CO oxidation over hexameric copper nanocluster catalyst supported on carboxyl-functionalised MWCNT at high temperatures, Chem. Eng. J. 389 (2020) 124399.

[84] G. Bond, Source of the catalytic activity of gold nanoparticles, Gold Bull. 43 (2010) 88–93.

[85] G.J. Wu, N.J. Guan, L.D. Li, Low temperature CO oxidation on Cu-Cu_2O/TiO_2 catalyst prepared by photodeposition, Catal. Sci. Technol. 1 (2011) 601–608.

[86] N. Li, Q.-Y. Chen, L.-F. Luo, W.-X. Huang, M.-F. Luo, G.-S. Hu, J.-Q. Lu, Kinetic study and the effect of particle size on low temperature CO oxidation over Pt/TiO_2 catalysts, Appl. Catal. B: Environ. 142–143 (2013) 523–532.

[87] D.B. Pedersen, S. Wang, S.H. Liang, Charge-Transfer-Driven Diffusion Processes in Cu@Cu-Oxide Core-Shell Nanoparticles: Oxidation of 3.0±0.3 nm Diameter Copper Nanoparticles, J. Phys. Chem. C 112 (2008) 8819–8826.

[88] K. Borgohain, N. Murase, S. Mahamuni, Synthesis and Properties of Cu_2O quantum particles, J. Appl. Phys. 92 (2002) 1292–1297.

[89] W.U. Khan, S.S. Chen, D.C.W. Tsang, W.Y. Teoh, X. Hu, F.L.Y. Lam, A.C.K. Yip, Catalytically active interfaces in titania nanorod-supported copper catalysts for CO oxidation. Nano Res. 13 (2020) 533–542.

[90] R. van den Berg, J. Zecevic, J. Sehested, S. Helveg, P.E. de Jongh, K.P. de Jong, Impact of the synthesis route of supported copper catalysts on the performance in the methanol synthesis reaction, Catal. Today 272 (2016) 87–93.

[91] S. Zhao, H.R. Yue, Y.J. Zhao, B. Wang, Y.C. Geng, J. Lv, S.P. Wang, J.L. Gong, X.B. Ma, Chemoselective synthesis of ethanol via hydrogenation of dimethyl oxalate on Cu/SiO_2: Enhanced stability with boron dopant, J. Catal. 297 (2013) 142–150.

[92] T. Popa, G. Xu, T.F. Barton, M.D. Argyle, High temperature water gas shift catalysts with alumina, Appl. Catal. A-Gen. 379 (2010) 15–23.

[93] N. Mammen, L. Spanu, E.C. Tyo, B. Yang, A. Halder, S. Seifert, M.J. Pellin, S. Vajda, S. Narasimhan, Reversing Size-Dependent Trends in the Oxidation of Copper Clusters through Support Effects, Eur. J. Inorg. Chem. (2018) 16–22.

[94] T.J. Huang, D.H. Tsai, CO oxidation behavior of copper and copper oxides, Catal. Lett. 87 (2003) 173–178.

[95] C.-H. Tu, A.-Q. Wang, M.-Y. Zheng, X.-D. Wang, T. Zhang, Factors influencing the catalytic activity of SBA-15-supported copper nanoparticles in CO oxidation, Appl. Catal. A: Gen. 297 (2006) 40–47.

[96] Y. Tang, L. Dong, C. Deng, M. Huang, B. Li, H. Zhang, In situ FT-IR investigation of CO oxidation on CuO/TiO_2 catalysts, Catal. Commun. 78 (2016) 33–36.

[97] I.H. Chowdhury, S. Ghosh, S. Basak, M.K. Naskar, Mesoporous $CuO\text{-}TiO_2$ microspheres for efficient catalytic oxidation of CO and photodegradation of methylene blue, J. Phy. Chem. Solids 104 (2017) 103–110.

[98] A.M. Abdel-Mageed, O.M. Yaghi, B. Rungtaweevoranit, M. Parlinska-Wojtan, X. Pei, O.M. Yaghi, R.J. Behm, Highly Active and Stable Single-Atom Cu Catalysts Supported by a Metal-Organic Framework, J. Am. Chem. Soc. 141 (2019) 5201–5210.

[99] E.M.C. Alayon, J. Singh, M. Nachtegaal, M. Harfouche, J.A. van Bokhoven, On highly active partially oxidized platinum in carbon monoxide oxidation over supported platinum catalysts, J. Catal. 263 (2009) 228–238.

[100] P.J. Berlowitz, C.H. Peden, D.W. Goodman, Kinetics of carbon monoxide oxidation on single-crystal palladium, platinum, and iridium, J. Phys. Chem. 92 (1988) 5213–5221.

[101] M.S. Chen, Y. Cai, Z. Yan, K.K. Gath, S. Axnanda, D.W. Goodman, Highly active surfaces for CO oxidation on Rh, Pd, and Pt, Surf. Sci. 601 (2007) 5326–5331.

[102] E.D. Park, J.S. Lee, Effects of pretreatment conditions on CO oxidation over supported Au catalysts, J. Catal. 186 (1999) 1–11.

[103] Y. Zhou, Z. Wang, C. Liu, Perspective on CO oxidation over Pd-based catalysts, Catal. Sci. Technol. 5 (2015) 69–81.

[104] Y. Li, Y. Yu, J.-G. Wang, J. Song, Q. Li, M. Dong, C.-J. Liu, CO oxidation over graphene supported palladium catalyst, Appl. Catal. B 125 (2012) 189–196.

Table and Figure Captions

Table 1. CO chemisorption of TiO_2-supported CuNC catalysts before the reaction.

Table 2. Quantitative results of CO- and O_2-TPD for *the* xCT catalysts.

Table 3. Comparison of the literature and the current work on CO oxidation over Cu/TiO_2 catalysts.

Fig. 1. Cu2p XPS spectra of the fresh 0.15CT, 0.75CT and 5CT catalysts.

Fig. 2. (a) CO-TPD profiles of the fresh 0.15CT, 0.75CT and 5CT catalysts; (b) O_2-TPD profiles of the fresh 0.15CT and 0.75CT catalysts.

Fig. 3. (a) CO conversion versus temperature for the xCT catalysts [x = 0.15 − 5 *wt*.% Cu]; (b) Turnover frequency versus time-on-stream for the xCT catalysts [x = 0.15 − 5 *wt*.% Cu].

Fig. 4. Reaction rates as a function of (a) CO and (b) O_2 partial pressures, and (c) the Arrhenius plot of CO oxidation over the 0.15CT (hollow triangles) and 0.75CT catalysts (filled circles).

Fig. 5. Initial reaction rate (IRR) versus initial partial pressure of CO for 0.15CT and 0.75CT catalysts.

Table 1. CO chemisorption of TiO_2-supported CuNC catalysts before the reaction.

Sample	CO adsorbed amount [cm^3 STP]	Cu dispersion [%]	Cu surface area [$m^2/g_{cat.}$]	Cu surface area [m^2/g_{Cu}]	Average particle diameter [nm]
0.15CT	0.0851	59.1	0.572	381.1	1.77
0.75CT	0.0081	10.8	0.526	70.1	9.59
5CT	0.0226	5.1	1.64	32.8	20.5
Spent 0.15CT	0.0731	53	0.513	341.9	1.97 (13.1)*
Spent 0.75CT	0.0042	4.9	0.318	31.8	21.1 (26.3)*
Spent 5CT	0.0051	1.7	0.533	10.7	63.1 (42.5)*

*Average copper oxide (Cu_2O) crystallite size obtained from Scherrer equation

Table 2. Quantitative results of CO- and O_2-TPD for the xCT catalysts.

Sample	CO uptake [mmol/g]			O_2 uptake [mmol/g]
	LTR	HTR	Total	
0.15CT	0.103	0.179	0.282	0.177
0.75CT	0.135	0.226	0.361	0.194
5CT	0.226	0.277	0.503	-

Table 3. Comparison of the literature and the current work on CO oxidation over Cu/TiO_2 catalysts.

Catalyst	Conditions	Rate ($\times 10^{-5}$ $mol_{CO}/s \cdot g_{Cu}$)	Ref.
$1\%Cu_6/Al_2O_3$	CO/O_2 = 1:10 v/v, Tr = 400 °C, F_{total} = 5 $mL \cdot min^{-1}$, m = 100 mg	2.68	78
$1\%Cu_6/MWCNT_{COOH}$		2.53	
$1\%Cu_6/MWCNT_{Pristine}$		2.31	

Cu/SBA-15-chl-Calc400	CO/O_2 = 1:1 v/v, Tr = 200 °C, F_{total} = 20 mL·min^{-1}, m = 60 mg	2.87	91
Cu/SBA-15-chl-Calc500		4.18	
Cu/SBA-15-chl-Calc700		2.13	
5CuO/TiO_2 (A)	CO/O_2 = 1.6:20.8 v/v, Tr = 200 °C, F_{total} = 20 mL·min^{-1}, m = 40 mg	3.81	92
5CuO/TiO_2 (A+R)		8.57	
CuO/TiO_2	CO/O_2 = 1:20 v/v, Tr = 200 °C, F_{total} = 40 mL·min^{-1}, m = 50 mg	4.80	93
Cu/UiO-66	CO/O_2 = 1:1 v/v, Tr = 180 °C, F_{total} = 30 mL·min^{-1}, m = 120 mg	2.40	94
Cu/UiO-66	CO/O_2 = 1:21 v/v, Tr = 250 °C, F_{total} = 30 mL·min^{-1}, m = 120 mg	6.05	
0.15CT	CO/O_2 = 1:10 v/v, Tr = 200 °C, F_{total} = 20 mL·min^{-1}, m = 200 mg	5.06	This work
0.3CT		2.53	
0.75CT		1.01	
5CT		0.15	

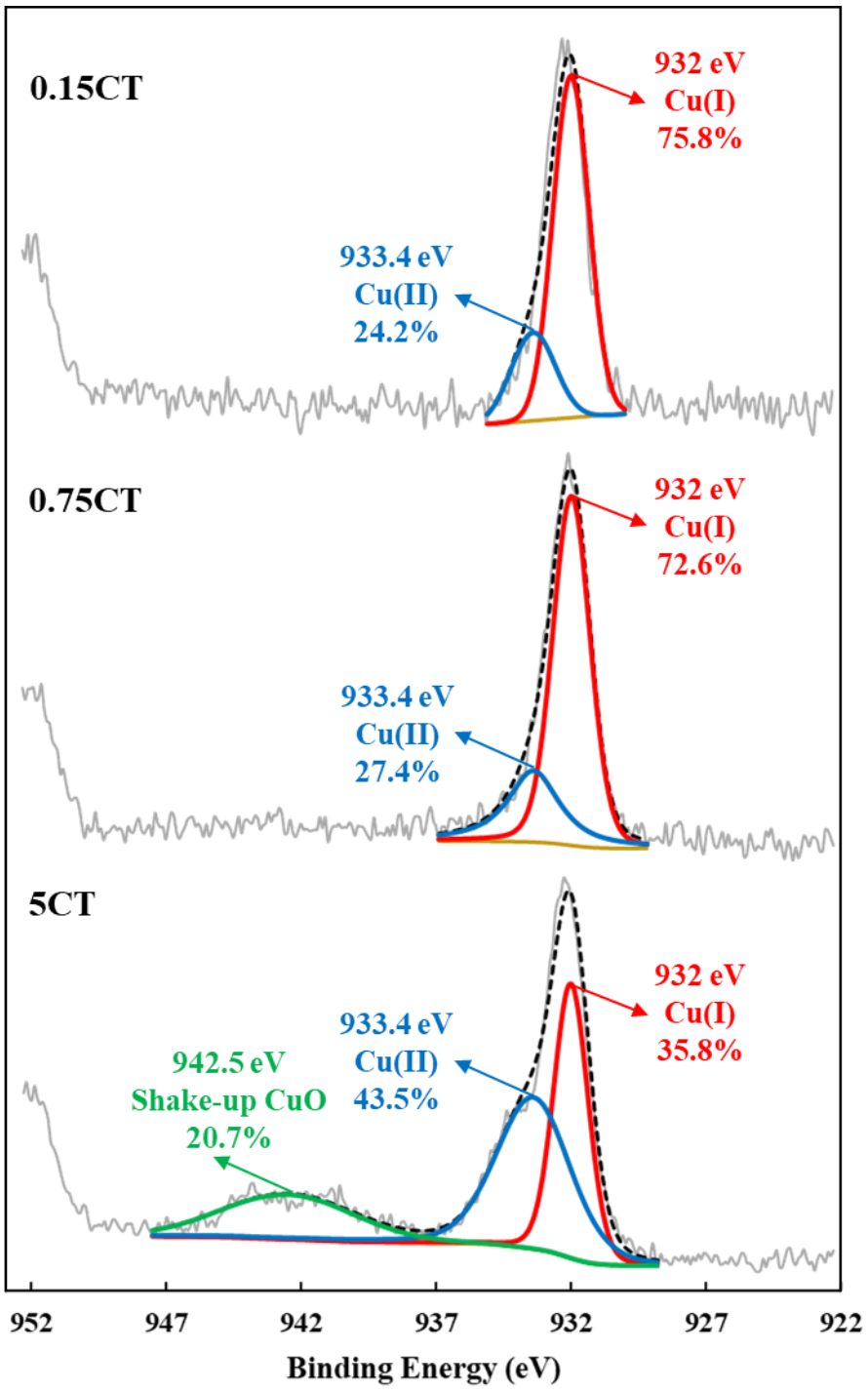

Fig. 1. Cu2p XPS spectra of the fresh 0.15CT, 0.75CT and 5CT catalysts.

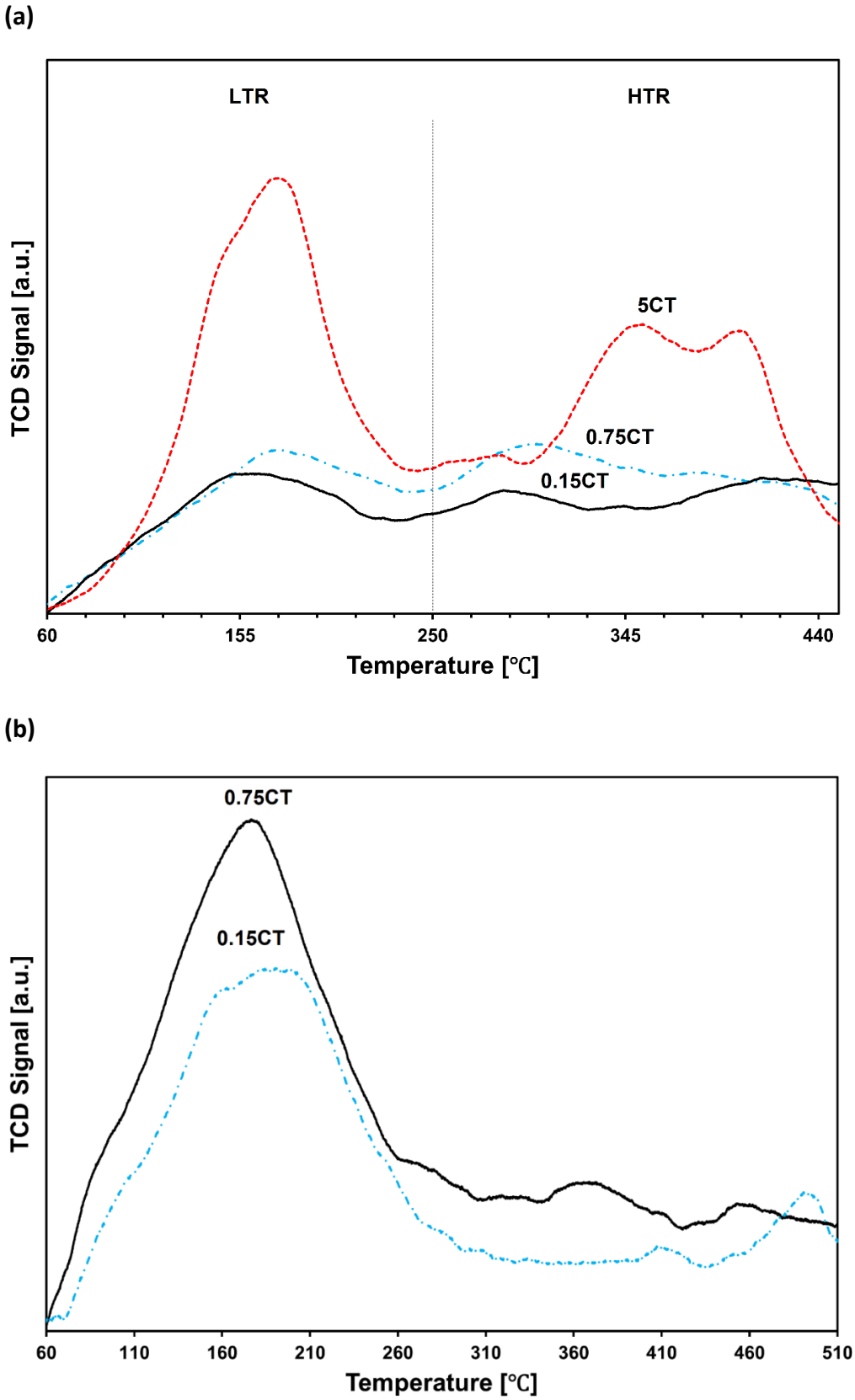

Fig. 2. (a) CO-TPD profiles of the fresh 0.15CT, 0.75CT and 5CT catalysts; (b) O_2-TPD profiles of the fresh 0.15CT and 0.75CT catalysts.

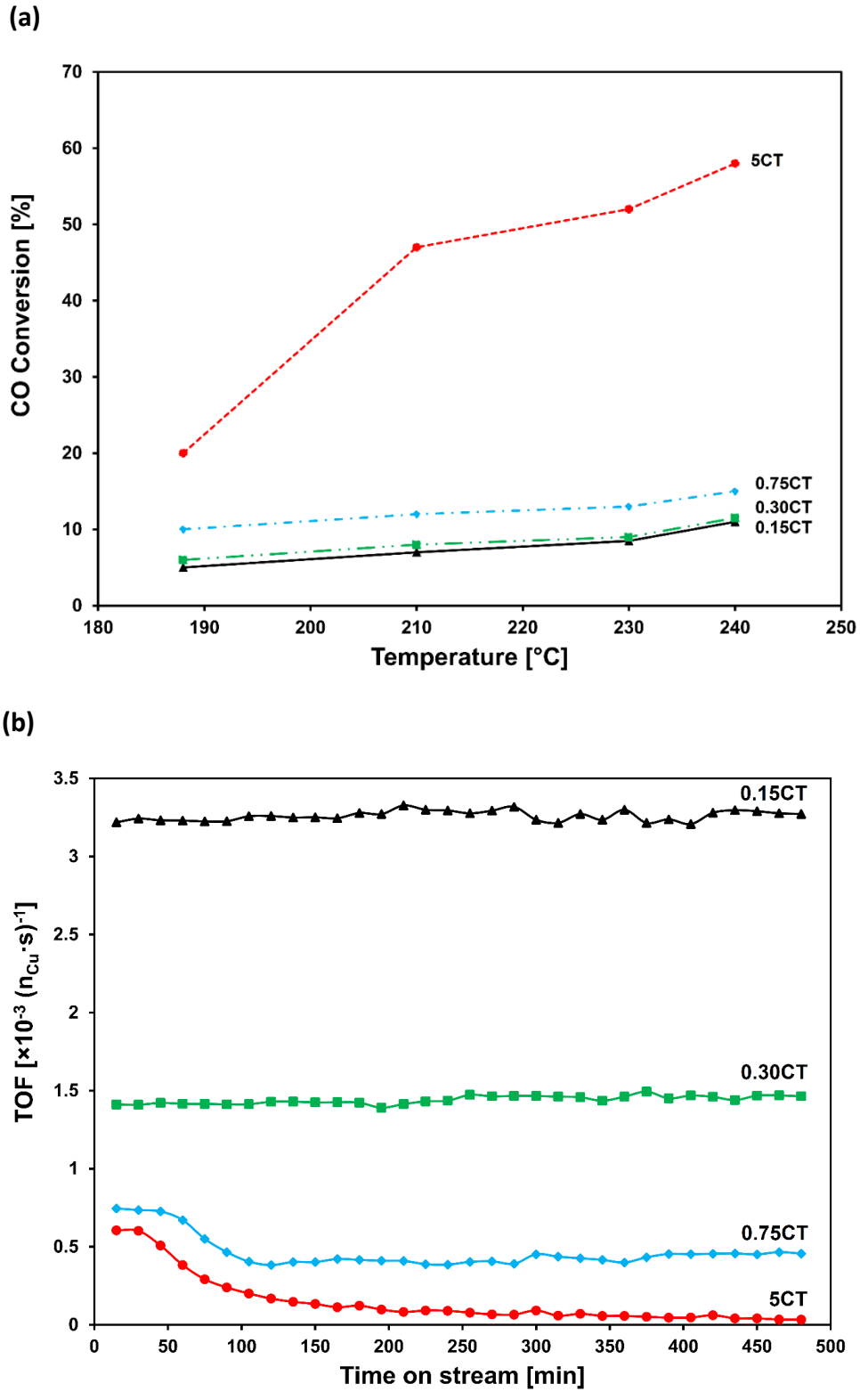

Fig. 3. (a) CO conversion versus temperature for the xCT catalysts [x = 0.15 − 5 *wt.*% Cu]; (b) Turnover number versus time-on-stream for the xCT catalysts [x = 0.15 − 5 *wt.*% Cu; T = 200°C, GHSV = 6000 ml/h.$g_{cat.}$, CO = 1 kPa, O_2 = 10 kPa balanced with He].

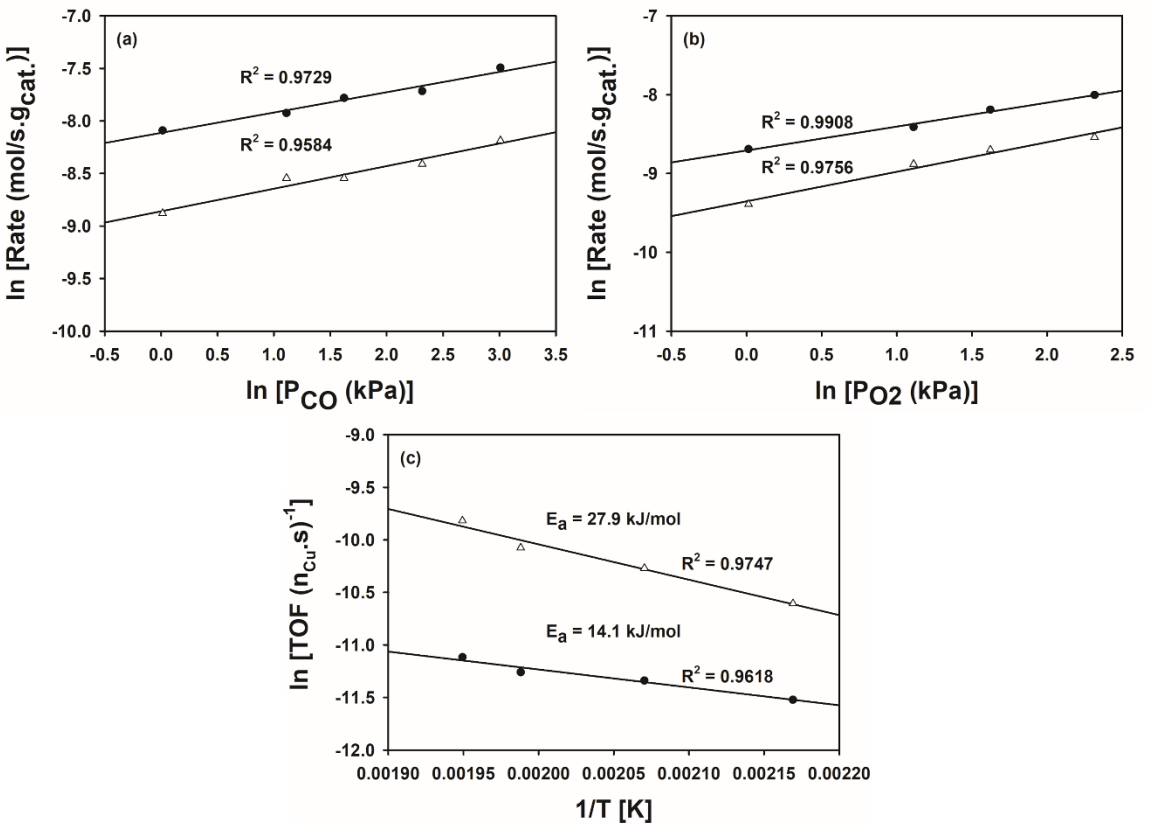

Fig. 4. Reaction rates as a function of (a) CO and (b) O_2 partial pressures, and (c) the Arrhenius plot of CO oxidation over the 0.15CT (filled circles) and 0.75CT catalysts (hollow triangles).

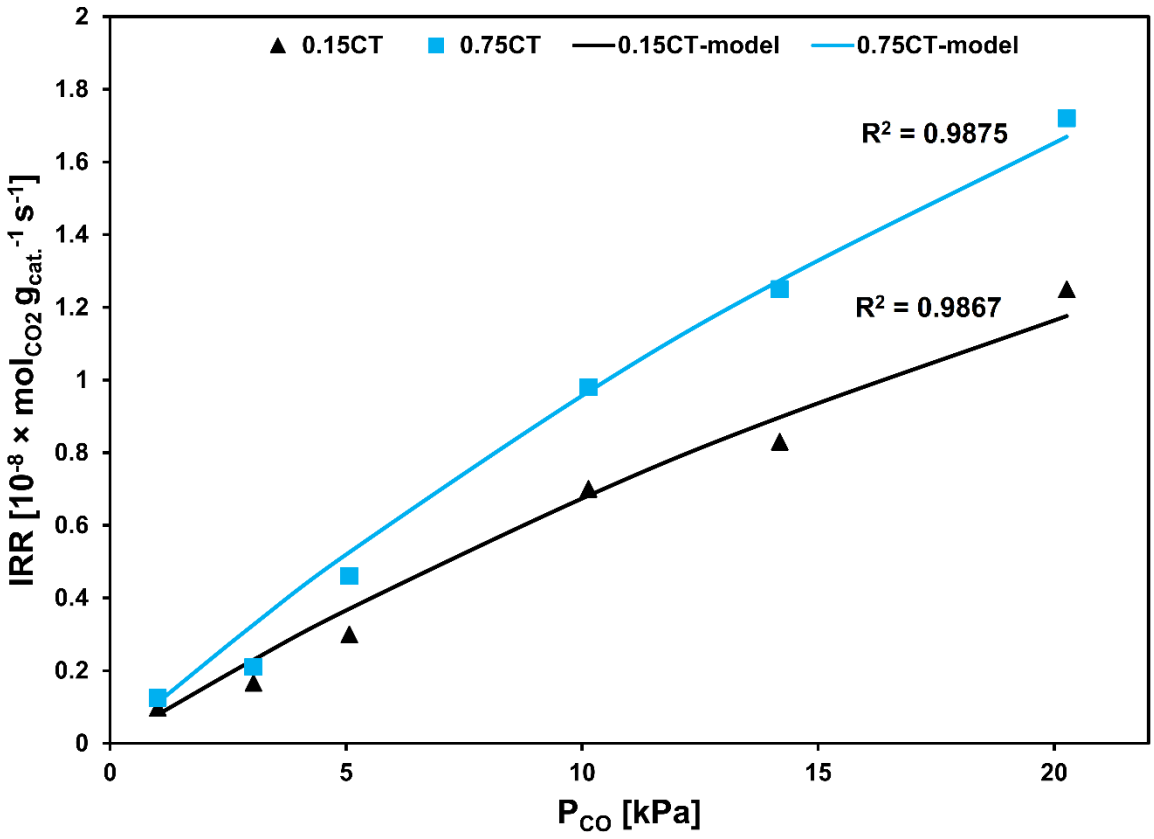

Fig. 5. Initial reaction rate (IRR) versus initial partial pressure of CO for 0.15CT and 0.75CT catalysts.